



Rate Coefficients for Dielectronic Recombination of Carbon-like $^{40}\text{Ca}^{14+}$

W. Q. Wen^{1,2} , Z. K. Huang¹, S. X. Wang³, N. Khan^{1,2}, H. B. Wang¹, C. Y. Chen⁴, C. Y. Zhang⁴, S. Preval⁵, N. R. Badnell⁶,
W. L. Ma³, D. Y. Chen¹, X. Liu¹, D. M. Zhao¹, L. J. Mao^{1,2}, J. Li¹, X. M. Ma¹, M. T. Tang¹, D. Y. Yin¹, W. Q. Yang¹,
Y. J. Yuan^{1,2} , J. C. Yang^{1,2}, L. F. Zhu³ , and X. Ma^{1,2,7} 

¹ Institute of Modern Physics, Chinese Academy of Sciences, 730000, Lanzhou, People's Republic of China; wenweiqiang@impcas.ac.cn, x.ma@impcas.ac.cn

² University of Chinese Academy of Sciences, 100049, Beijing, People's Republic of China

³ Hefei National Laboratory for Physical Sciences at Microscale, Department of Modern Physics, University of Science and Technology of China, 230026, Hefei, People's Republic of China

⁴ Shanghai EBIT Laboratory, Institute of Modern Physics, Fudan University, Shanghai 200433, People's Republic of China

⁵ Department of Physics and Astronomy, University of Leicester, University Road, Leicester LE1 7RH, UK

⁶ Department of Physics, University of Strathclyde, Glasgow G4 0NG, UK

⁷ ExtreMe Matter Institute EMMI, GSI Helmholtzzentrum für Schwerionenforschung, D-64291 Darmstadt, Germany

Received 2020 April 26; revised 2020 October 4; accepted 2020 October 14; published 2020 December 9

Abstract

Dielectronic recombination (DR) rate coefficients for carbon-like $^{40}\text{Ca}^{14+}$ forming nitrogen-like $^{40}\text{Ca}^{13+}$ have been measured using the electron–ion merged-beam technique at the heavy-ion storage ring CSRm at the Institute of Modern Physics in Lanzhou, China. The measured DR rate coefficients in the energy range from 0 to 92 eV cover most of the DR resonances associated with $2s^22p^2 \rightarrow 2s^22p^2$ and $2s^22p^2 \rightarrow 2s2p^3$ core transitions ($\Delta N = 0$). Theoretical calculations of the DR cross sections were carried out by using two different state-of-the-art atomic theoretical techniques, multiconfiguration Breit–Pauli (MCBP) code AUTOSTRUCTURE and relativistic configuration interaction code FAC, to compare with the experimental rate coefficients. The theoretical calculations agree with the experimental results at collision energy higher than 10 eV. However, significant discrepancies of resonance energies and strengths can be found at collision energy below 8 eV. Temperature-dependent plasma recombination rate coefficients were derived from the measured DR rate coefficients in the energy range from 0.1 to 1000 eV and compared with the recommended atomic data from the literature. The theoretical data of Gu et al. and Zatsarinny et al. are 30% lower than the experimental results at the temperatures of photoionized plasmas, but have a very good agreement at the temperatures of collisionally ionized plasmas. Other previously published theoretical data of Jacobs et al. and Mazzotta et al. by using Burgess formula and LS-coupling calculations significantly underestimate the plasma rate coefficients in the low temperature range. The present results comprise a set of benchmark data suitable for astrophysical modeling.

Unified Astronomy Thesaurus concepts: [Atomic spectroscopy \(2099\)](#); [Spectroscopy \(1558\)](#); [Atomic data benchmarking \(2064\)](#); [Atomic physics \(2063\)](#)

1. Introduction

Various atomic processes occur in astrophysical plasmas, such as electron impact ionization, electron collision excitation, and electron–ion recombination (Beiersdorfer 2003; Savin 2007a; Smith & Brickhouse 2014). The astrophysical plasmas are divided into two forms, photoionized plasma and collisionally ionized plasma, corresponding to different temperature ranges. Emission features generated from these plasmas are the most important and precise diagnostic sources to deduce the plasmas properties, such as density, temperature, as well as the elemental abundances (Kallman & Palmeri 2007). In order to investigate the properties of astrophysical plasmas, space-based X-ray observatories, such as XMM-Newton and Chandra, have been launched to detect X-ray emissions from different astrophysical objects (Paerels & Kahn 2003). These spectra have resulted in major scientific breakthroughs (Kaastra 2017), such as the discovery of an unresolved transition array (UTA) between 16 and 17 Å in the soft X-ray spectra of active galactic nuclei (AGNs; Sako et al. 2001) and the detection of X-rays from a Kuiper Belt object (Lisse et al. 2017). In order to extend the investigations to the distant universe and even very weak sources with much higher time resolution and higher spectral resolution, several future X-ray observatories are under preparation or at the proposal phases, including the X-ray grating spectrometer

explorer (Arcus; Smith et al. 2016), X-Ray Imaging and Spectroscopy Mission (XRISM; Tashiro et al. 2018), and Advanced Telescope for High ENergy Astrophysics (ATHENA; Nandra et al. 2013), as well as The Lynx X-ray Surveyor (Lynx; Özel 2018; Gaskin et al. 2019). These missions will cover an energy bandpass of ~ 0.1 –10 keV, a range that includes strong lines from L-shell and M-shell of many abundant elements, with a resolved power hundred times higher than the previous x-ray observatories of Chandra and XMM-Newton.

It should be noted that accurate plasma models and atomic data are essential for diagnostics of various plasma and understanding of the high-quality spectra that are recorded by the spectrometers on board the future missions (Kaastra 2017; Mao et al. 2019). There are three widely used atomic databases for modeling the collisionally ionized plasmas, including AtomDB (Foster et al. 2012), CHIANTI (Dere et al. 2019), and SPEX (Kaastra et al. 1996). Two plasma modeling codes are used for modeling photoionized plasmas, called CLOUDY (Ferland et al. 1998a) and XSTAR (Bautista & Kallman 2001). All of these plasma models and atomic databases have played a significant role in understanding the universe with the observed data from space-based observatories. However, with the new unprecedented high-resolution X-ray satellite Hitomi, the observed X-ray spectrum from the Perseus galaxy cluster challenges the current astrophysical collisionally ionized

plasma models that are widely used in the community (Aharonian et al. 2018, 2017). Since the input atomic data in the current plasma models are mostly from theoretical data (Kallman & Palmeri 2007), the Hitomi results show that substantial updates of atomic databases and targeted laboratory measurements are urgently needed before the next-generation X-ray satellite missions (Aharonian et al. 2018).

The importance of dielectronic recombination (DR) in the solar corona plasma was recognized by Burgess for the first time in 1964 (Burgess 1964). Afterwards, DR is regarded as an important atomic process in plasma physics. However, very few DR experimental work exists for the L-shell B-, C-, N-, O-, F-, and Ne-like ions as well as for all of the M-shell isoelectronic sequences (Savin 2007a). For high-temperature DR rates theory and experiment agree to within $\sim 35\%$ for the few systems studied; however, low-temperature DR rates are theoretically and computationally challenging, and the difficulties in atomic-structure calculations limit the accuracy of DR resonance energies for center-of-mass collision energies less than 1–3 eV (Savin 2007b). As a result, there can be up to a factor of 2 spread between calculated rates with different theories (Savin et al. 2000). The lack of reliable low-temperature DR rates for most third-row and higher-Z elements is the dominant uncertainty in the ionization balance in photoionization equilibrium (Ferland et al. 1998b; Ferland 2003). In order to provide reliable DR rate coefficients for use in plasma modeling, the storage ring DR experiments combined with the new calculations with the AUTOSTRUCTURE code and the FAC code have made huge progress in the past few decades. Storage ring DR experiments of highly charged iron have been performed with almost all of the charge states for Fe^{7+} to Fe^{22+} (Savin 2007a; Schippers 2012). Following the first paper to describe the calculation goals and methodology (Badnell et al. 2003), a series of the papers have been published based on the calculations by the AUTOSTRUCTURE code, and the calculated data are collected into the recent database CHIANTI (Dere et al. 2009, 2019). By comparison of these calculations and the storage ring experiments, DR rate coefficients for carbon-like and oxygen-like ions have been identified as the most urgent needs for astrophysical applications, and therefore precision measurements of the DR rate coefficients of these ions that are abundant in astrophysical plasmas to benchmark the theories are required.

Calcium is an abundant element in the solar corona and also in high-temperature astrophysical plasmas. Emission lines from highly charged calcium ions play an important role for diagnostics and modeling in astrophysical plasmas as well as fusion plasmas (Del Zanna & Mason 2018; Träbert et al. 2018). For a C-like Ca^{14+} ion, the previous observations were mostly from solar flare and solar wind based on the lines that are largely in the EUV range. These EUV lines are usually from the transitions within the $2s^22p^2-2s^22p^2$ and $2s^22p^2-2s2p^3$ configurations. The spectral lines of 555 Å and 1098 Å from $2s^22p^2-2s^22p^2$ transitions of Ca xv were measured and identified by the Solar Ultraviolet Measurements of Emitted Radiation spectrometer on the Solar and Heliospheric Observatory (SOHO). With the Skylab observation, the ratios of the 181.90 or 215.37 Å lines versus the resonance EUV line at 200.98 Å are excellent density diagnostics at high densities of solar flares (Dere et al. 1979). This Skylab observation of Ca xv emission lines to derive the electron density was later on confirmed by a new data analysis and a measurement from the TEXT tokamak plasma (Keenan et al. 1988, 2003). The Ca xv

181.90/200.98 Å ratio was also investigated by the observations of solar coronal emission lines with the Extreme-Ultraviolet Imaging Spectrometer (Culhane et al. 2007) on Hinode spacecraft (Kosugi et al. 2007), as discussed by Warren et al. (2008) and Del Zanna (2008), and several Ca xv emission lines at EUV range are formed at about 4MK and the electron density measurements at these temperatures are potentially important for understanding the coronal heating mechanism. In addition to the EUV emission lines, transitions of C-like Ca xv within the $2s^22p^2-2s^22p3d$ configurations that fall into the soft X-rays are also useful for electron density diagnostics, as shown by Brown et al. (1986). It can be found in Table 1 that lines from Ca xv of transitions within the $2s^22p^2-2s^22p3d$ configurations are around ~ 0.5 keV (~ 22 Å), which are within the observation range of the future X-ray observatories. These lines are very important for density diagnostics of ionized outflows in active galactic nuclei, as discussed by Mao et al. (2017). Since the emission lines of X-rays from Ca xv are very close in wavelength, high-resolution X-ray spectrometers, such as Arcus (Smith et al. 2016) and Lynx (Gaskin et al. 2019; Özel 2018), will resolve them. As a result, the emission lines at the X-ray range from C-like Ca xv will be detected for diagnostic of electron density at a high-temperature range in different astrophysical objects. In order to provide more atomic data of C-like Ca xv to be used for astrophysical modeling, a summary of the spectral lines for Ca xv can be found in the atomic data table compiled by Bhatia & Doschek (1993), and systematic calculations of energy levels and transition rates of C-like ions including Ca xv can be found in Jönsson et al. (2011), Ekman et al. (2014), and Wang et al. (2014). Very recently, emission lines from highly charged calcium ions including Ca xv in the EUV and X-ray range were investigated in the tokamak plasmas for the astrophysical applications (Träbert et al. 2018).

Here, we report on absolute DR rate coefficients of C-like calcium from a storage ring experiment at the Heavy Ion Research Facility at Lanzhou (HIRFL) at Lanzhou, China (Yuan et al. 2013). As compared with many other experimental techniques, such as electron beam ion traps (Beiersdorfer 2003) and tokamak plasmas (Wang et al. 1988), the electron-ion merged-beam method at heavy-ion storage rings provides an ideal experimental platform for DR precision spectroscopy of highly charged ions (HCIs) particularly at the low-energy range. The details about storage ring DR experiments with HCIs can be found in the reviews (Schuch & Böhm 2007; Müller 2008; Brandau et al. 2015; Schippers 2015) and the references cited therein.

We have measured DR rate coefficients for C-like Ca^{14+} forming N-like Ca^{13+} over the collision energy range of 0–92 eV. The expected electron-ion recombination channels can be written as follows:

$$\begin{aligned} & \text{Ca}^{14+}(2s^22p^2[{}^3P_0]) + e^- \\ & \rightarrow \begin{cases} \text{Ca}^{13+}(2s^22p^2[{}^3P_0]nl) + \gamma, \text{ RR}; \\ \text{Ca}^{13+}(2s^22p^2[{}^3P_{1,2}; {}^1D_2; {}^1S_0]nl)^{**} \rightarrow \text{Ca}^{13+} + \gamma, \text{ DR}; \\ \text{Ca}^{13+}(2s2p^3[{}^5S_2^o; {}^3D_{2,1,3}^o; {}^3P_{1,2,3}^o; {}^1D_2^o; {}^3S_1^o; {}^1P_1^o]nl)^{**} \\ \quad \rightarrow \text{Ca}^{13+} + \gamma, \text{ DR}; \\ \text{Ca}^{13+}(2p^4[{}^3P_{2,1,0}; {}^1D_2; {}^1S_0]nl)^{**} \rightarrow \text{Ca}^{13+} + \gamma, \text{ TR}. \end{cases} \end{aligned} \quad (1)$$

Here, γ is the decay photons. RR means radiative recombination, where a free electron is captured into a bound state of the ion with simultaneous emission of a photon. DR is a resonant process, in which a free electron is captured into a bound state of

Table 1
Energy Levels and Associated Lifetimes of $^{40}\text{Ca}^{14+}$ Ions

Level	Energy		Lifetime (s)
	NIST (eV)	Wang et al. (2014)	
		(eV)	
$1s^2 2s^2 2p^2 \ ^3P_0$	0.0000	0.00000	8
$1s^2 2s^2 2p^2 \ ^3P_1$	2.1770	2.17805	1.063[-02]
$1s^2 2s^2 2p^2 \ ^3P_2$	4.4539	4.45434	1.274[-02]
$1s^2 2s^2 2p^2 \ ^1D_2$	13.465	13.4569	7.293[-04]
$1s^2 2s^2 2p^2 \ ^1S_0$	24.508	24.5188	1.076[-04]
$1s^2 2s 2p^3 \ ^5S_2^o$	34.21	34.2788	1.782[-07]
$1s^2 2s 2p^3 \ ^3D_2^o$	61.580	61.5640	2.049[-10]
$1s^2 2s 2p^3 \ ^3D_1^o$	61.691	61.6720	1.860[-10]
$1s^2 2s 2p^3 \ ^3D_3^o$	62.021	62.0058	2.371[-10]
$1s^2 2s 2p^3 \ ^3P_0^o$	72.125	72.1140	8.403[-11]
$1s^2 2s 2p^3 \ ^3P_1^o$	72.256	72.2441	8.462[-11]
$1s^2 2s 2p^3 \ ^3P_2^o$	72.614	72.6013	9.085[-11]
$1s^2 2s 2p^3 \ ^3S_0^o$	90.370	90.3640	1.595[-11]
$1s^2 2s 2p^3 \ ^1D_2^o$	90.465	90.4393	3.085[-11]
$1s^2 2s 2p^3 \ ^1P_1^o$	100.970	100.946	1.941[-11]
$1s^2 2p^4 \ ^3P_2$	137.319	137.244	2.663[-11]
$1s^2 2p^4 \ ^3P_1$	140.579	140.517	2.510[-11]
$1s^2 2p^4 \ ^3P_0$	141.338	141.279	2.489[-11]
$1s^2 2p^4 \ ^1D_2$	148.176	148.071	4.331[-11]
$1s^2 2p^4 \ ^1S_0$	167.489	167.391	2.108[-11]

Note. Numbers in brackets represent powers of 10. The NIST data are from Kramida et al. (2019).

an ion and, simultaneously, an initially bound electron is excited through a resonant interaction, forming a doubly excited intermediate state. Subsequently, this doubly excited state decays via photon emission resulting in the stabilization of the recombined ion due to the excitation energy below its ionization threshold, this is called radiative stabilization. In trielectronic recombination (TR), the capture of one free electron leads to the resonant excitation of two core electrons. Then, a triply excited intermediate level is formed; finally, these excited states decay by photon emission to complete this process. The excitation energies and lifetimes associated with channels belonging to DR and TR processes with $\Delta n = 0$ transitions are listed in Table 1.

In storage ring DR experiments of C-like ions, the DR resonance strengths and energies for C-like Fe^{20+} have been measured at the heavy-ion storage ring TSR and compared with different theoretical calculations (Savin et al. 2003). Later on, DR experiments of C-like Mg^{6+} (Lestinsky et al. 2012) and Ar^{12+} (Mahmood et al. 2020) were performed at the TSR and the CSRm, respectively. Here, we report the first measurement of the DR rate coefficients of C-like Ca^{14+} forming N-like Ca^{13+} . The paper is organized as follows: Section 2 presents the experimental procedures and the data analysis. Section 3 gives a brief description of the theoretical codes of AUTO-STRUCTURE and FAC. The experimental merged-beam DR rate coefficients as well as plasma recombination rate coefficients are presented and compared with literature data in Section 4. A conclusion is made in Section 5.

2. Experimental Technique and Data Analysis Methods

The experiment was performed by the ion–electron beams merging technique on the main cooler storage ring (CSRm) at

the Institute of Modern Physics (IMP) in Lanzhou, China. The procedures for DR measurements at the CSRm have already been described in detail elsewhere (Huang et al. 2015; Khan et al. 2018; Wang et al. 2018). Several electron–ion recombination experiments related to astrophysical and fusion plasmas have been investigated very recently (Huang et al. 2020, 2018; Wang et al. 2019). Here, we provide only a brief description of the DR experiment with C-like Ca^{14+} at the CSRm.

C-like $^{40}\text{Ca}^{14+}$ ions were generated by a Superconducting Electron Cyclotron Resonance (SECR) ion source (Sun et al. 2020) and accelerated at a Sector Focused Cyclotron (SFC), and then a beam of $6.22 \text{ MeV u}^{-1} \ ^{40}\text{Ca}^{14+}$ ions were injected into the CSRm. The typical current of the stored ions was around $70 \mu\text{A}$ corresponding to 1.46×10^8 ions. The beam lifetime was about 50 s. In the electron cooler section of the CSRm, the cold electron beam was merged with the ion beam. The cold electron beam was obtained by adiabatically expanding from the 125 mT magnetic field at the electron-gun area to 39 mT at the electron-cooling area. The diameter of the electron beam was approximately 50 mm at the cooling section, with an electron density of $n_e = 2.75 \times 10^5 \text{ cm}^{-3}$. The cold electron beam was used to cool the ion beam and was employed as an electron target in DR measurement. By fitting the DR spectrum of Ca^{14+} , the obtained transversal and longitudinal electron temperatures were $k_B T_{\perp} = 12.4(2) \text{ meV}$ and $k_B T_{\parallel} = 0.33(1) \text{ meV}$, respectively, which are consistent with the temperatures obtained in the DR experiment of B-like Ar^{13+} at the CSRm (Huang et al. 2020), but differ from the machine design parameters (Huang et al. 2015). Since the electron density distribution along the beam radius can be varied by adding a special control electrode to the conventional gun at the electron cooler of the CSRm (Bocharov et al. 2004), the investigation of the electron temperature will be carried out systematically by more DR experiments as well as by simulations in further studies.

After injection, the ion beam was first electron-cooled for 3 s by setting the electron beam to the cooling energy. As a result, the momentum spread and the diameter of the ion beam were decreased. The diameter of the ion beam reached approximately 5 mm before data taking. This cooling time is much longer than the lifetimes of the various Ca^{14+} metastable levels as listed in Table 1. Therefore, all of the collected data are from the ground state of the ions during this storage ring experiment. We started data collection after this precooling scheme with every beam injection at the CSRm. The electron beam energy was scanned by the electron energy detuning system to provide a relative collision energy between electrons and ions. Beam position monitors were employed to diagnose the relative ion beam and electron beam positions to ensure both beams parallel in the cooler section. During the experiment, the recombined Ca^{13+} ions were magnetically separated from the Ca^{14+} beam in the first bending magnet downstream of the electron cooler and recorded with a movable scintillator particle detector of approximately 100% efficiency (Wen et al. 2013). At the same time, the ion beam current was measured by a DC current transformer (DCCT); the electron beam current and cathode high voltage were recorded accordingly. Additionally, the longitudinal momentum spread and the revolution frequency of the ion beam were measured by a Schottky pick-up for the off-line data analysis (Wu et al. 2013).

In storage ring experiments, the absolute DR recombination rate coefficients can be deduced from the background + RR subtracted recombination counting rate as a function of collision energy E_{rel} (Bernhardt et al. 2011):

$$\alpha(E) = \frac{R}{N_i n_e (1 - \beta_e \beta_i)} \cdot \frac{C}{L}. \quad (2)$$

Here, R is the recombination count rate, N_i is the number of stored ions, n_e is the density of the electron beam, the velocities of the electron beam and ion beam are $\beta_e = v_e/c$ and $\beta_i = v_{ion}/c$, and $L = 4.0$ m and $C = 161.0$ m denote the length of the effective interaction section and the circumference of the storage ring.

The center-of-mass collision energies between electrons and ions were calculated using the added detuning voltage at the electron cooler. The space-charge effect and drag force were taken into account to deduce accurate collision energies (Huang et al. 2015). For the DR experiment of Ca^{14+} , the high voltage added on the cathode is 3.456 kV at the cooling point. The scanning mode was operated with 190 ms cooling and 10 ms tuning in the collision energy range from 0 to 25 eV. For a collision energy of 25–80 eV, the scanning mode was operated with 190 ms cooling and 20 ms tuning. In order to obtain a stable condition for DR experiment at the collision energies higher than 80 eV, the scanning mode was operated with 250 ms cooling and 40 ms tuning. It should be noted that the scanning step keeps 1 volt for all measurements, which corresponds to a collision energy of 0.005 eV at 0.1 eV, 0.05 eV at 10 eV, and 0.14 eV at 50 eV, respectively.

In the experiment, recombination involves capturing a free electron into a Rydberg level n , and the recombined ions have to experience motional electric fields as they travel through the CSRm magnets. These electric fields can ionize the recombined ions when an electron is recombined into high- n Rydberg levels of the ion. Therefore, the recombined ion with principal quantum number $n > n_{cutoff}$ will be field-ionized and cannot be detected. The estimated critical quantum number is $n_{cutoff} = 77$ as described in our previous paper (Huang et al. 2018).

The uncertainty in the experimental rate coefficients at the CSRm is estimated to be around 30% (at a 1σ confidence level). It mainly originates from uncertainties of the electron density distribution profile, the electron and ion beam currents, the length of the electron–ion interaction region, the position of the ion beam in this profile, and also the statistical errors that are the smallest among them.

3. Theoretical Methods

To compare with the measured DR rate coefficients of Ca^{14+} , two state-of-the-art theoretical atomic codes, AUTOSTRUCTURE (Badnell 2011) and FAC (Gu 2003, 2008), were employed to carry out theoretical calculations. The details of the calculations for the DR process implemented by AUTOSTRUCTURE have already been described elsewhere and the references cited therein (Badnell et al. 2003). The AUTOSTRUCTURE code is based on the lowest-order perturbation theory, and is able to calculate energy levels, radiative/autoionization rates, oscillator strengths, and many other quantities using semirelativistic kappa-averaged wave functions. For calculation of DR cross sections, both the electron–electron and electron–photon interactions are treated to first order (Badnell 2011). The energy levels, radiative rates, and

autoionization rates are calculated independently, and then used to compute the DR resonance profiles to generate the final state level-resolved and the total DR rate coefficients. The FAC code (Gu 2008) is a relativistic and configuration interaction atomic-structure program. The FAC code has already been used for calculating various atomic collisional and radiative processes, including atomic energy levels, autoionization and radiative decay rates. The DR process is treated as two independent steps in the FAC calculation, namely, dielectronic capture and radiative/autoionization decay of the doubly excited states. The DR cross sections are obtained for the final states by considering all possible electronic transitions from doubly excited states. The detailed calculation processes can be found in the literature (Chen et al. 2010). In the present FAC calculations, the doubly and triply excited intermediate states $1s^2 2l^i n l$ ($n \leq 75$, $l \leq 12$) are considered. And the electron correlations among different complexes $1s^2 2l^i n l$ ($n \leq 7$, $l \leq 6$) are explicitly considered. For $n \geq 8$ states, a simple hydrogenic scaling law is used for the resonance energies, the autoionization rates, and the radiative decay rates. The optimal radial potential is optimized on the $1s^2 2l^i$ configurations of the recombining ion. The MBPT method (Gu 2005) is employed to calculate the low- n resonance energies. The Hilbert space of the system is divided into two subspaces, including a model space and an orthogonal space; the $1s^2 2l^i n l$ ($n \leq 7$, $l \leq 6$) configurations are contained in the model space, and all possible configurations that are generated from single or double excitations of the model space are involved in the orthogonal space. For single and double excitations the maximum principal quantum numbers are 150 and 65, respectively, and the maximum orbital quantum number is 20. The detailed description of calculations could refer to our previous work (Wang et al. 2016), where the similar MBPT calculations are performed, and the comparison with NIST values are discussed in detail. The agreement of the present MBPT energy levels and the previous results are on the level of 0.01%. In order to calibrate the calculated DR spectrum, the core excited energies have been adjusted by the spectroscopic values from the NIST atomic spectra database (Kramida et al. 2019) for both theoretical calculations. The detailed comparison for calculation of DR cross sections between the AUTOSTRUCTURE and FAC codes are described in the references (Savin et al. 2006, 2003).

The DR rate coefficients as well as the plasma recombination rate coefficients can be obtained by convolution of the calculated recombination cross section $\sigma(v)$ with the appropriate electron energy distribution,

$$\alpha(E) = \langle v\sigma \rangle = \int v\sigma(v)f(v)d^3v. \quad (3)$$

Here, $f(v)$ is the velocity distribution of the electron beam. For comparison with the experimentally derived merged-beam rate coefficients, $f(v)$ is a flattened Maxwellian distribution with the longitudinal and transverse temperatures $k_B T_{\parallel}$ and $k_B T_{\perp}$. For comparison with the experimentally derived temperature-dependent plasma rate coefficients, $f(v)$ is an isotropic Maxwellian distribution determined by the electron temperature T_e in the plasmas (Kilgus et al. 1992; Savin et al. 2000).

4. Results and Discussion

4.1. Merged-beams DR Rate Coefficients

Figure 1 shows the experimentally measured DR rate coefficients of C-like $^{40}\text{Ca}^{14+}$, as well as the theoretical results

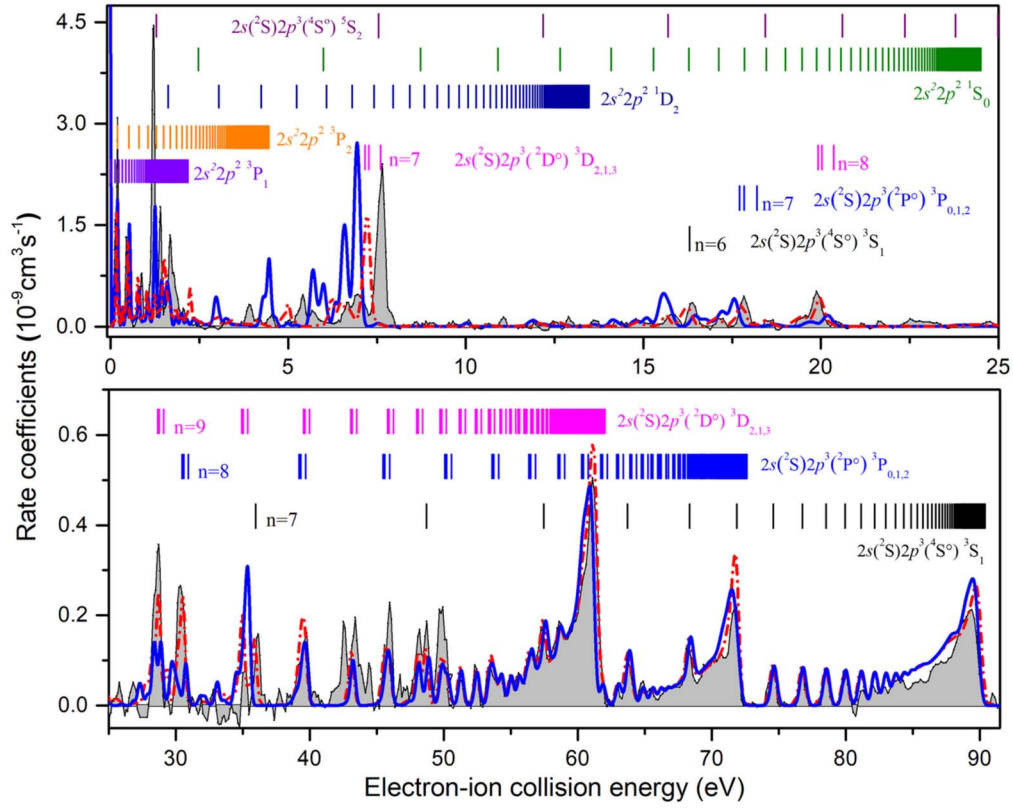


Figure 1. Experimental DR rate coefficients of C-like Ca^{14+} as a function of relative energy (gray area). DR series associated with $2s^2 2p^2 \rightarrow 2s^2 2p^2$ and $2s^2 2p^2 \rightarrow 2s^2 2p^3$ core excitations ($\Delta N = 0$) are observed, and their resonance positions are indicated by short bars of different colors. Theoretical DR rate coefficients from the AUTOSTRUCTURE and FAC codes are shown by the short-dashed-dotted red line and the blue solid lines, respectively. Both theoretical curves contain the recombination into Rydberg states with the principal quantum number up to $n = 1000$ and $n = 300$, respectively, which is called the field-ionization-free recombination rate coefficient.

from the AUTOSTRUCTURE (short-dashed-dotted red line) and the FAC (blue solid line) calculations. The theoretical rate coefficients from AUTOSTRUCTURE and the FAC were obtained by convoluting the calculated DR resonance cross sections with the velocity distribution of the electron beam as described in Section 3. The fitting of the first 10 resonance peaks for relative energies below 0.6 eV using a flattened Maxwellian function is shown in Figure 2 (Kilgus et al. 1992); we obtained longitudinal and transversal electron temperatures of $k_B T_{\parallel} = 0.33(1)$ meV and $k_B T_{\perp} = 12.4(2)$ meV, respectively. The numbers in parentheses correspond to the uncertainties from the fit with one standard deviation. The obtained experimental energy resolution of FWHM is better than 0.04 eV at collision energies around 0.2 eV, 0.2 eV at 10 eV, and 1.5 eV at 60 eV, respectively.

In general, the resonance positions of DR for each Rydberg state can be estimated by the Rydberg formula:

$$E_{res} = E_{exc} - R_y \left(\frac{Q}{n} \right)^2, \quad (4)$$

where E_{exc} is the core transition energy of the ions, R_y is the Rydberg constant, and Q is the ionic charge. The vertical bars in Figure 1 indicate the calculated Rydberg resonance series of the doubly excited intermediate levels.

In Figure 1, the measured DR rate coefficients with a collision energy range of 0–92 eV cover almost all of the DR resonances associated with $2s^2 2p^2 \rightarrow 2s^2 2p^2$ and $2s^2 2p^2 \rightarrow 2s^2 2p^3$ ($\Delta N = 0$) core excitations. Three strong resonance series belong to

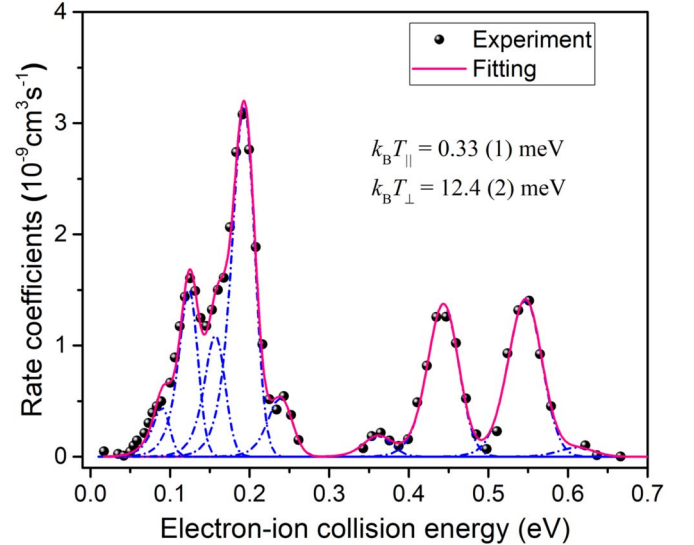


Figure 2. The fitting of the first nine experimental resonance peaks at relative energies below 0.7 eV, as described in Schippers et al. (2004) and Huang et al. (2018). The experimental DR rate coefficient and peak fitting are shown by the black filled symbols and the solid red line. The individual fitted peaks are shown by dashed-dotted blue lines. The fit resulted in $k_B T_{\parallel} = 0.33(1)$ meV and $k_B T_{\perp} = 12.4(2)$ meV.

$2s^2 2p^3 (^3D_{2,1,3}^o)nl$ and $2s^2 2p^3 (^3P_{0,1,2}^o)nl$; $2s^2 2p^3 (^3S_1)nl$ can be identified with the help of the Rydberg formula, and the series limits are around 62 eV, 72 eV, and 90 eV, respectively. Other series limits are not clearly observed in the DR rate coefficients.

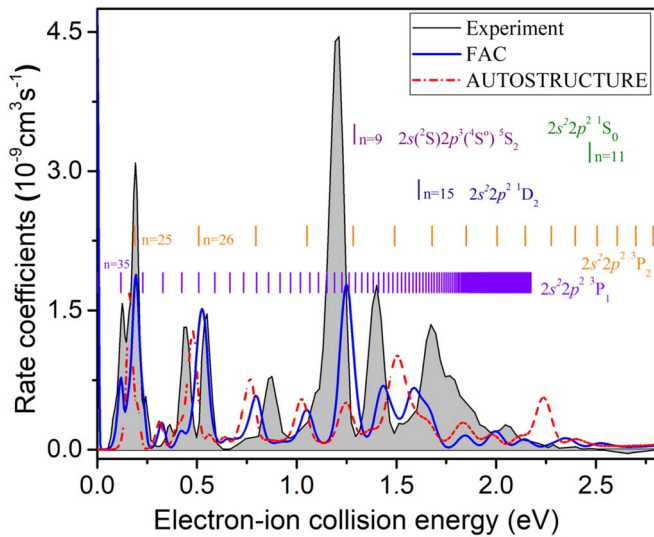


Figure 3. Same as Figure 1, but with a more detailed comparison at a low-energy range.

There is a large discrepancy in resonance positions and intensities at a collision energy below 8 eV between the theories and experiment. A more detailed comparison between the experiment and calculations at a low collision energy range is shown in Figure 3. A very strong peak around 1.2 eV cannot be explained by theories. The strong electron–electron correlation effects at a low-energy range challenges precision calculation in the current theories.

From 8 eV to 25 eV, there are only a few peaks observed. A good agreement has been found between the experimental result and the AUTOSTRUCTURE calculation; however, the intensities and positions of resonances are not reproduced by FAC calculation. From 25 eV to 50 eV, many excited peaks appear in the DR spectrum; both calculations provide reasonable agreement in DR resonance positions, but they cannot well reproduce the resonance intensities. Between 50 eV and 92 eV, as seen in Figure 1, a very good agreement can be found between the experiment and theories. For high principal quantum number n , the correlation between the captured electron and the core electrons are very weak, and the accurate calculation of the resonance positions and strengths can be very well achieved. The discrepancy between experimental and theoretical results at the series limits around 62 eV, 72 eV, and 90 eV are due to the field-ionization effects of the storage ring experiment. As shown in Figure 1, the theoretical curves from AUTOSTRUCTURE and FAC contain the recombination into states with the principal quantum number up to $n = 1000$ and $n = 300$, respectively, which is called the field-ionization-free recombination rate coefficient. However, the electrons recombined into states with a principal quantum number higher than the $n_{\text{cutoff}} = 75$ will be field-ionized in a magnetic field during the storage ring DR experiment at the CSRm as discussed in Section 2 and described in detail in Huang et al. (2018) and Wang et al. (2019). In order to obtain the field-ionization-free plasma rate coefficients to compare with the existing published data, we replaced the experimental DR rate coefficients from 60 eV to 92 eV by the AUTOSTRUCTURE results. It is to be noted that the contribution of the dielectronic capture into the resonance levels with $n > 1000$ is very small and can be neglected.

4.2. Plasma Recombination Rate Coefficients

The procedure to obtain the temperature-dependent plasma recombination rate coefficients from DR rate coefficients has been discussed in Section 3. The field-ionization-free plasma rate coefficients were deduced by using the same procedure as described by Huang et al. (2018) and Schippers et al. (2001). Figures 4(a) and (b) show the comparison of the experimentally derived plasma rate coefficients with the present theoretical data from the AUTOSTRUCTURE and FAC codes as well as the theoretical data from the literature, respectively. The temperature range of 0.1 to 1000 eV includes the photoionized and collisionally ionized plasmas for C-like Ca^{14+} . The boundaries corresponding to the two plasmas are illustrated by vertical dashed lines. They mark the temperature region where the concentration of C-like Ca is higher than 10% of its maximum value (Kallman & Bautista 2001; Bryans et al. 2009).

Figure 4(a) demonstrates that the calculated data from FAC has a good agreement with the experimental results in the temperature range including photoionized and collisionally ionized plasmas, but shows a significant difference in the temperature range from 0.1 to 2 eV. The calculated data from the AUTOSTRUCTURE code in this work give a good agreement over the temperature range from 30 to 1000 eV; however, they underestimate the plasma rate coefficients in the temperature range from 0.1 to 20 eV as compared with the experimental data.

The DR plasma rate coefficients calculated by Mazzotta et al. (1998) and Jacobs et al. (1980), as shown by full circles and stars in Figure 4(b), are very different from the experimental data (gray area). At the temperature range from 0.1 to 20 eV, these two theoretical data significantly underestimate the rate coefficients. However, the calculated data from Mazzotta et al. (1998) and Jacobs et al. (1980) included not only the transitions for $\Delta N = 0$, but also included the transition from $\Delta N = 1$, which was not measured in the present experiment. Therefore, the calculated data from these two papers are more than 80% higher than the experimental data at ~ 300 eV in the temperature range of collisionally ionized plasma.

The calculated data from Zatsarinny et al. (2004) and Gu (2003), using the AUTOSTRUCTURE code and the FAC code, are shown by full squares and full triangles in Figure 4(b), respectively. It can be found that only these two theoretical calculations show important contributions to plasma rate coefficients in the low-temperature range. At around 1 eV, the calculated data from Zatsarinny et al. (2004) are 70% lower than the experimental data, but the data from Gu (2003) are in a good agreement with the experiment. In the temperature range from 2.6 to 34.5 eV, where C-like Ca is expected to be abundant in photonionized plasmas, the calculated data from Zatsarinny et al. (2004) and Gu (2003) are more than 30% lower than the experimental results. At a temperature of about 400 eV where Ca^{14+} is supposed to be abundant in collisionally ionized plasmas, the calculated data from Zatsarinny et al. (2004) have a very good agreement with the experimental data, and the theoretical data of Gu (2003) are 20% lower than the experimental results. It should be noted that agreement within 2% is found between the current calculation by the AUTOSTRUCTURE code and the data from Zatsarinny et al. (2004). However, the MBPT methods were employed to obtain more accurate level energies in the present FAC calculation; as a result, the current theoretical data from the FAC code show a

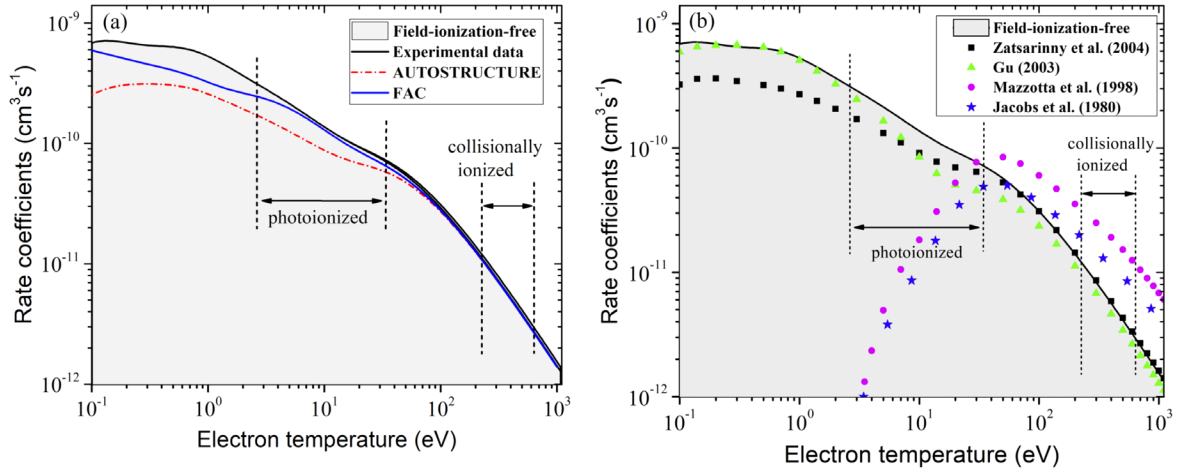


Figure 4. Plasma recombination rate coefficients of C-like Ca^{14+} . (a) Comparison of plasma rate coefficients between experimental results (black solid line) and the present calculations by the AUTOSTRUCTURE and FAC codes. (b) Comparison of field-ionization-free plasma recombination rate coefficients (light gray area) with theoretical data available in the literature. Full squares and full triangles show rate coefficients by Zatsarinny et al. (2004) and Gu (2003). Data from Mazzotta et al. (1998) and Jacobs et al. (1980) are shown by full circles and stars, respectively. The temperature ranges associated with photoionized and collisionally ionized plasmas in which the Ca^{14+} concentration is higher than 10% of its maximum abundance are indicated (Bryans et al. 2009; Kallman & Bautista 2001).

better agreement with experimental data in the temperature ranges covering photoionized plasma and collisional plasma than the previously calculated data from Gu (2003).

In order to facilitate the use of the experimentally measured results in plasma modeling, the $\Delta N = 0$ resonant plasma rate coefficients were parameterized by fitting with the function

$$\alpha(T_e) = T_e^{-3/2} \sum_i c_i \times \exp\left(-\frac{E_i}{T_e}\right). \quad (5)$$

The fitted parameters of c_i and E_i are listed in Table 2. The present calculated data are also fitted with this function for convenient comparison to the experimental and previous theoretical results. The experimental and calculated data can be reproduced within 2% at a energy range from 0.1 eV up to 1000 eV by these fitted parameters.

5. Conclusions

We have measured DR rate coefficients of C-like Ca^{14+} forming N-like Ca^{13+} and compared the results with theoretical calculations. The experimental DR resonances associated with $\Delta N = 0$ ($2s^22p^2 \rightarrow 2s^22p^2$ and $2s^22p^2 \rightarrow 2s2p^3$) within the energy range of 0–92 eV were studied and identified using the Rydberg formula. The AUTOSTRUCTURE code and the FAC code are employed for calculations. A good agreement was found for DR resonance positions and strengths at collision energies higher than 8 eV. However, a significant discrepancy was found at a low collision energy range, similar to the previous results from storage ring DR experiments of multi-electron highly charged ions.

The plasma recombination rate coefficients were deduced from the experimental DR rate coefficients in the temperature range from 0.1 to 1000 eV and compared with existing literature data. This temperature range covers both the photoionized and collisionally ionized plasmas in which Ca^{14+} ions are abundant. At the temperature range of photoionized plasmas, the most recent results of Gu (2003) and Zatsarinny et al. (2004) are $\sim 30\%$ smaller than the experimental ones. For a temperatures range within ~ 220 –630 eV of the collisionally ionized plasmas, these two

Table 2
Fitted Parameters of Plasma Recombination Rate Coefficients for DR of Ca^{14+} Forming Ca^{13+} ($\Delta N = 0$)

No.	Experiment	AUTOSTRUCTURE	FAC
c_1	2.580E-1	8.415E-2	4.118E-1
c_2	3.419E-1	2.490E-1	3.831E-1
c_3	3.310E-2	1.595E-2	3.255E-2
c_4	1.036E+0	7.902E-1	1.202E+0
c_5	3.323E+0	3.437E+0	2.562E+0
c_6	1.151E-1	5.371E-2	6.694E-2
c_7	1.230E-2	4.500E-3	7.300E-3
E_1	5.855E+0	4.199E+0	6.092E+0
E_2	1.184E+1	8.813E+0	1.602E+1
E_3	7.104E-1	5.807E-1	7.386E-1
E_4	3.233E+1	2.755E+1	4.365E+1
E_5	7.018E+1	6.868E+1	7.703E+1
E_6	1.502E+0	1.515E+0	1.962E+0
E_7	1.753E-1	1.788E-1	1.368E-1

Note. The experimental results are field-ionization-free DR plasma rate coefficients as described in the text, the AUTOSTRUCTURE results for $n_{\max} = 1000$, and the FAC results for $n_{\max} = 300$. The units of c_i and E_i are $10^{-8} \text{ cm}^3 \text{ s}^{-1}$ and eV, respectively.

calculated data agree well within 20% of the experimental ones. However, the calculated data from Mazzotta et al. (1998) and Jacobs et al. (1980) significantly underestimate the rate coefficients as compared with the present experimental results in the photoionized temperature range. Our experimental DR data of Ca^{14+} ions thus provide a benchmark for use in astrophysical and laboratory plasma modeling.

This work is partly supported by the National Key R&D Program of China under grant No. 2017YFA0402300, the National Natural Science Foundation of China through No. U1932207, No. 11904371, No. U1732133, and No. 11674066, the Strategic Priority Research Program of Chinese Academy of Sciences No. XDB34020000 and No. XDB21030300, and Key Research Program of Frontier Sciences, CAS, grant No. QYZDY-SSW-SLH006. We thank S. Schippers for the fruitful

discussion of data analysis. W.Q.W. is grateful for the support by the Youth Innovation Promotion Association CAS. N.R.B. acknowledges the support of the UK APAP Network STFC grant ST/R000743/1. The authors would like to thank the staff of the Accelerator Department for smooth running of the CSR accelerator complex.

ORCID iDs

W. Q. Wen  <https://orcid.org/0000-0001-5266-3058>

Y. J. Yuan  <https://orcid.org/0000-0002-1761-9040>

L. F. Zhu  <https://orcid.org/0000-0002-5771-0471>

X. Ma  <https://orcid.org/0000-0001-9831-0565>

References

- Aharonian, F., Akamatsu, H., Akimoto, F., et al. 2017, *Natur*, **551**, 478
- Aharonian, F., Akamatsu, H., Akimoto, F., et al. 2018, *PASJ*, **70**, 13
- Badnell, N. R. 2011, *CoPhC*, **182**, 1528
- Badnell, N. R., O'Mullane, M., Summers, H., et al. 2003, *A&A*, **406**, 1151
- Bautista, M., & Kallman, T. 2001, *ApJS*, **134**, 139
- Beiersdorfer, P. 2003, *ARA&A*, **41**, 343
- Bernhardt, D., Brandau, C., Harman, Z., et al. 2011, *PhRvA*, **83**, 020701
- Bhatia, A., & Doschek, G. 1993, *ADNDT*, **53**, 195
- Bocharov, V., Buble, A., Boimelstein, Y., et al. 2004, *NIMPA*, **532**, 144
- Brandau, C., Kozhuharov, C., Lestinsky, M., et al. 2015, *PhyS*, **2015**, 014022
- Brown, W. A., Bruner, M. E., Acton, L. W., et al. 1986, *ApJ*, **301**, 981
- Bryans, P., Landi, E., & Savin, D. W. 2009, *ApJ*, **691**, 1540
- Burgess, A. 1964, *ApJ*, **139**, 776
- Chen, C.-Y., Wang, K., Huang, M., et al. 2010, *JQSRT*, **111**, 843
- Culhane, J. L., Harra, L. K., James, A. M., et al. 2007, *SoPh*, **243**, 19
- Del Zanna, G. 2008, *A&A*, **481**, L69
- Del Zanna, G., & Mason, H. E. 2018, *LRSP*, **15**, 5
- Dere, K., Mason, H., Widing, K., et al. 1979, *ApJS*, **40**, 341
- Dere, K. P., Landi, E., Young, P. R., et al. 2009, *A&A*, **498**, 915
- Dere, K. P., Zanna, G. D., Young, P. R., et al. 2019, *ApJS*, **241**, 22
- Ekman, J., Jönsson, P., Gustafsson, S., et al. 2014, *A&A*, **564**, A24
- Ferland, G., Korista, K., Verner, D., et al. 1998a, *PASP*, **110**, 761
- Ferland, G. J. 2003, *ARA&A*, **41**, 517
- Ferland, G. J., Korista, K. T., Verner, D. A., et al. 1998b, *PASP*, **110**, 761
- Foster, A. R., Ji, L., Smith, R. K., et al. 2012, *ApJ*, **756**, 128
- Gaskin, J. A., Swartz, D., Vikhlinin, A. A., et al. 2019, *JATIS*, **5**, 021001
- Gu, M. F. 2003, *ApJ*, **590**, 1131
- Gu, M. F. 2005, *ApJS*, **156**, 105
- Gu, M. F. 2008, *CaJPh*, **86**, 675
- Huang, Z. K., Wang, S. X., Wen, W. Q., et al. 2020, *XRS*, **49**, 155
- Huang, Z. K., Wen, W. Q., Wang, H. B., et al. 2015, *PhST*, **2015**, 014023
- Huang, Z. K., Wen, W. Q., Xu, X., et al. 2018, *ApJS*, **235**, 2
- Jacobs, V., Davis, J., Rogerson, J., et al. 1980, *ApJ*, **239**, 1119
- Jönsson, P., Rynkun, P., & Gaigalas, G. 2011, *ADNDT*, **97**, 648
- Kaastra, J., Mewe, R., & Nieuwenhuijzen, H. 1996, *UV and X-ray Spectroscopy of Astrophysical and Laboratory Plasmas*, **411**
- Kaastra, J. S. 2017, *AN*, **338**, 146
- Kallman, T., & Bautista, M. 2001, *ApJS*, **133**, 221
- Kallman, T. R., & Palmeri, P. 2007, *RvMP*, **79**, 79
- Keenan, F., Aggarwal, K., Berrington, K., et al. 1988, *ApJ*, **327**, 473
- Keenan, F., Aggarwal, K., Katsiyannis, A., et al. 2003, *SoPh*, **217**, 225
- Khan, N., Huang, Z.-K., Wen, W.-Q., et al. 2018, *ChPhC*, **42**, 064001
- Kilgus, G., Habs, D., Schwalm, D., et al. 1992, *PhRvA*, **46**, 5730
- Kosugi, T., Matsuzaki, K., Sakao, T., et al. 2007, *SoPh*, **243**, 3
- Kramida, A., Ralchenko, Y., Reader, J., et al. 2019, *Atomic Spectra Database, NIST Standard Reference Database 78, Version 5.8*, <https://physics.nist.gov/asd>
- Lestinsky, M., Badnell, N. R., Bernhardt, D., et al. 2012, *ApJ*, **758**, 40
- Lisse, C. M., McNutt, R. L., Wolk, S. J., et al. 2017, *Icar*, **287**, 103
- Mahmood, S., Huang, Z. K., Wen, W. Q., et al. 2020, *JPhB*, **53**, 085004
- Mao, J., Kaastra, J., Mehdipour, M., et al. 2017, *A&A*, **607**, A100
- Mao, J., Mernier, F., Kaastra, J. S., et al. 2019, *JInst*, **14**, C07012
- Mazzotta, P., Mazzitelli, G., Colafrancesco, S., et al. 1998, *A&AS*, **133**, 403
- Müller, A. 2008, *AAMOP*, **55**, 293
- Nandra, K., Barret, D., Barcons, X., et al. 2013, arXiv:1306.2307
- Özel, F. 2018, *NatAs*, **2**, 608
- Paerels, F. B. S., & Kahn, S. M. 2003, *ARA&A*, **41**, 291
- Sako, M., Kahn, S. M., Behar, E., et al. 2001, *A&A*, **365**, L168
- Savin, D., Badnell, N., Bartsch, T., et al. 2000, in *Atomic Data Needs for X-ray Astronomy*, ed. M. A. Bautista, T. R. Kallman, & A. K. Pradhan (Washington, DC: NASA), **143**
- Savin, D. W. 2007a, *JPhCS*, **88**, 012071
- Savin, D. W. 2007b, in *AIP Conf. Proc. 926, Atomic Processes in Plasma*, ed. J. D. Gillaspay, J. J. Curry, & W. L. Wiese (Melville, NY: AIP), **124**
- Savin, D. W., Gwinner, G., Griesser, M., et al. 2006, *ApJ*, **642**, 1275
- Savin, D. W., Kahn, S., Gwinner, G., et al. 2003, *ApJS*, **147**, 421
- Schippers, S. 2012, *JPhCS*, **388**, 012010
- Schippers, S. 2015, *NIMPB*, **350**, 61
- Schippers, S., Müller, A., Gwinner, G., et al. 2001, *ApJ*, **555**, 1027
- Schippers, S., Schnell, M., Brandau, C., et al. 2004, *A&A*, **421**, 1185
- Schuch, R., & Böhm, S. 2007, *JPhCS*, **88**, 012002
- Smith, R., Abraham, M., Allured, R., et al. 2016, *Proc. SPIE*, **9905**, 99054M
- Smith, R. K., & Brickhouse, N. S. 2014, *AAOMP*, **63**, 271
- Sun, L., Zhao, H. W., Lu, W., et al. 2020, *XRS*, **49**, 47
- Tashiro, M., Maejima, H., Toda, K., et al. 2018, *Proc. SPIE*, **10699**, 1069922
- Träbert, E., Beiersdorfer, P., Lepson, J. K., et al. 2018, *ApJ*, **865**, 148
- Wang, J.-S., Griem, H. R., Hess, R., et al. 1988, *PhRvA*, **38**, 4761
- Wang, K., Li, D. F., Liu, H. T., et al. 2014, *ApJS*, **215**, 26
- Wang, K., Si, R., Dang, W., et al. 2016, *ApJS*, **223**, 3
- Wang, S.-X., Huang, Z.-K., Wen, W.-Q., et al. 2019, *A&A*, **627**, A171
- Wang, S. X., Xu, X., Huang, Z. K., et al. 2018, *ApJ*, **862**, 134
- Warren, H. P., Feldman, U., & Brown, C. M. 2008, *ApJ*, **685**, 1277
- Wen, W. Q., Ma, X., Xu, W. Q., et al. 2013, *NIMPB*, **317**, 731
- Wu, J. X., Zang, Y. D., Nolden, F., et al. 2013, *NIMPB*, **317**, 623
- Yuan, Y. J., Yang, J. C., Xia, J. W., et al. 2013, *NIMPB*, **317**, 214
- Zatsarinsky, O., Gorczyca, T., Korista, K., et al. 2004, *A&A*, **417**, 1173